Materials Science Forum
ISSN: 1662-9752, Vol. 1191, pp 7-14
doi:10.4028/p-gydQM7

Submitted: 2025-09-10
Revised: 2026-01-26
Accepted: 2026-02-23
Online: 2026-05-19

Investigation of Mechanical Stress and Warpage in 200 mm Silicon Carbide Wafers: Implications for Production Scalability

Lin Dong[1,a*], Qiqi Wu[2,b] and Stefan Nufer[1,c]

[1]Robert Bosch GmbH, Tübinger Straße 123, 72762 Reutlingen, Germany

[2]Robert Bosch GmbH, 333 Fuquan (N.) Road, Shanghai 200335 P.R. China

[a]Lin.Dong2@de.bosch.com, [b]Qiqi.WU@cn.bosch.com, [c]Stefan.Nufer@de.bosch.com

Keywords: wafer warpage analysis, mechanical stress, photoelastic measurements, 200 mm SiC wafer technology.

Abstract. Controlling wafer warpage is critical for SiC power device fabrication on 200 mm substrates. Residual mechanical stress in bare SiC wafers is a major contributor to bow and warp. In this study, photoelastic measurements were employed to reveal distinct stress levels among wafers from different vendors, which reflect differences in crystal growth and wafering processes. By decomposing the stress into radial and tangential components, two dominant stress distribution modes—symmetric and asymmetric—were identified. The results demonstrate a clear correlation between residual mechanical stress and wafer warpage in 200 mm SiC substrates.

Introduction

Bosch is continuously expanding its semiconductor business in silicon carbide (SiC) chips by significantly expanding manufacturing facilities and scaling up 200 mm wafer production lines [1]. This growth is accompanied by the establishment of a diversified supplier portfolio, following a multi-sourcing and multi-location strategy. From a technical perspective, in addition to a deep understanding of substrate quality and supplier maturity, front-loaded requirements engineering is essential for ensuring the scalability of production.

In recent years, Bosch has focused on improving crystal defect characteristics; however, the large diameter wafer warpage control during the device manufacturing is now gaining increased attention. The overall shape of a substrate is typically defined by its bow and warp. As the wafer diameter increases from 150 mm to 200 mm, the influence of gravity on bow and warp values becomes more pronounced. According to SEMI standards for silicon wafers, which typically include diameters of 200 mm and 300 mm, the effects of gravity on bow and warp values can be estimated through experimental or mathematical methods [2-3]. However, for SiC wafers, particularly with the industry's initial adoption of 200 mm wafers, these topics have not been extensively explored.

The warpage of a wafer results from the overall mechanical stress state within the material, which can be induced during various manufacturing steps. Notably, the residual mechanical stress in the wafer due to SiC crystalline growth and wafering process can be a primary contributor to excessive bow and warp during device fabrication. Therefore, it is highly important to investigate residual mechanical stress in 200 mm SiC bare substrates and its impact on wafer warpage. We aim at establishing a monitoring method suitable for series production to control stress in incoming SiC wafers. Photoelastic measurement is a suitable method for assessing the stress levels in crystalline materials such as SiC and silicon wafers [4]. This paper focuses on Bosch's in-depth investigation of residual mechanical stress in SiC substrates and the stress-warpage correlation.

Experimental

We have investigated the warpage behavior and mechanical stress of multiple 200 mm n-type (0001) 4° off-cut 4H-SiC bare wafers produced from different vendors. The typical wafer thickness is 350 ± 25 µm. To ensure that the surface stress due to the sub-surface damage does not influence the measurements, the Si-face of all samples underwent chemical-mechanical polishing (CMP), and

the C-face was treated either by CMP or fine lapping. The wafer bow and warp measurements were conducted using E+H and FRT metrology tools, which employ 2-rod and 3-point supports, respectively.

Photoelastic stress analysis was performed using the Raphael Optech SV200 and ilis StrainScope Stepper 200, both of which enable non-destructive visualization of internal stress distributions [5-6]. Figure 1(a) shows the schematic diagram of the optical path. Light emitted from the source S_0 (630 nm for Raphael, 590 nm for ilis) first passes through a linear polarizer with a vibration direction along the y-axis. It then enters a quarter-wave plate $Q(\pi/4, \delta)$, whose fast axis is oriented at 45° to the polarizer, introducing a phase retardation δ to generate circularly polarized light. This light subsequently passes through the sample $M(\theta, \phi)$, where θ denotes the optical axis orientation and ϕ represents the phase retardation induced by internal stress. Finally, the transmitted light reaches the polarization-sensitive camera $P_i(\beta)$, which analyzes the polarization state at angle β (=0°, 45°, 90° and 135°) and records the intensity distribution. As described in Fig. 1(b), prior to photoelastic stress measurements, the sample holder was adjusted to ensure that the light beam propagated along the wafer's c-axis direction by considering 4H-SiC refractive index (n = 2.63) and off-cut angle to eliminate the natural birefringence phenomenon of 4H-SiC crystal. During the measurement, the whole sample area was scanned along a pre-determined path. The optical phase difference between ordinary and extraordinary light, along with the optical axis orientation (θ) was recorded. The stress was then calculated based on the stress-optic law below:

$$n_1 - n_2 = C(\sigma_1 - \sigma_2), \quad (1)$$

where n_1 and n_2 are the refractive index of fast and slow birefringence axis, respectively, and C is the photoelastic constant, which is -2.82×10^{-12} Pa^{-1} in this study [7]. σ_1 and σ_2 represent the principal stresses along the fast and slow axes. The fast axis corresponds to the direction of lower refractive index, while the slow axis corresponds to higher refractive index — thus $n_1 < n_2$. Given $C < 0$, this implies $\sigma_1 > \sigma_2$.

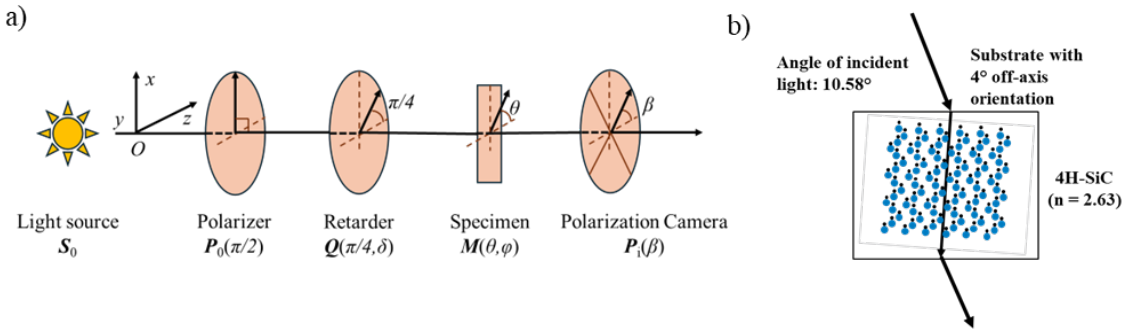

Fig. 1. (a) Schematic diagram of the instrument's optical path; (b) Schematic drawing of light beam alignment with the [0001] crystallographic orientation of 4H-SiC.

Results and Discussion

Photoelastic Stress Analysis. We first compared wafer stress results obtained from the Raphael Optech SV200 and the ilis StrainScope Stepper 200. Table 1 presents the measured stress values for the same group of SiC samples using both instruments. The observed deviation between the two tools correlates with ingot and most likely due to different beam alignment at the two measurements. Therefore, the results are highly comparable, indicating good consistency between the two measurement systems. Additionally, we also compared the photoelastic stress distributions obtained from the two instruments and confirmed that all key stress features were consistently reproduced in both maps.

To assess the stress characteristics of incoming substrates from various vendors, Figure 2 presents photoelastic stress distributions across 200 mm 4H-SiC wafers supplied by six different vendors. Although the investigation included a baseline of at least three wafers from three different ingots for

each supplier, with the sampling for two of the six suppliers being significantly more extensive, it was noted that wafers from a single source could still exhibit variations in stress patterns due to different growth runs or processing batches. Therefore, the wafers depicted in Fig. 2 are representative examples chosen to illustrate the most characteristic stress profile for each vendor. The stress levels vary significantly among vendors, both in terms of average stress values and spatial distribution. This variation reflects the influence of different crystal growth conditions, wafering techniques, and post-processing treatments employed by each supplier. Some wafers exhibit relatively uniform stress distributions, while others show pronounced asymmetries or localized stress concentrations. To better understand these patterns, the stress maps were further analyzed and grouped based on their symmetry characteristics. Despite the differences in stress patterns, the wafers can be broadly classified into two distinct groups. Figure 3 shows two typical stress distributions of 200 mm SiC wafers. In first column of average stress mapping, the top wafer exhibits an axisymmetric stress profile with the central region predominantly dark blue (stress near 0 MPa) transitioning to yellow and red at the wafer periphery (reaching approximately 20 MPa), indicative of a uniform thermal gradient and controlled cooling process. The white arrows in the average stress maps, representing the direction of the fast birefringence axis and principal stress, are constantly aligned along radial or tangential orientations, suggesting a highly symmetric stress field probably resulting from optimized crystal growth parameters, such as a low thermal gradient. In contrast, the bottom wafer displays an asymmetric stress distribution, with significant stress concentrations across both central and edge regions, and white arrows indicating a non-axisymmetric stress field. This asymmetry, potentially arising from non-uniform temperature gradients during growth or cooling, may elevate the risk of defects such as basal plane dislocation (BPD) or even cracking.

Table 1. Comparison of wafer stress results from Raphael Optech SV200 and ilis StrainScope Stepper 200, showing near-identical measurements.

Sample	Average Stress (MPa)		Comparison
	Raphael Optech SV200	ilis StrainScope Stepper 200	Stress Ratio (ilis/Raphael)
Ingot A / Wafer #08	2.90	2.91	1.00
Ingot A / Wafer #06	2.66	2.68	1.01
Ingot A / Wafer #03	2.46	2.50	1.01
Ingot B / Wafer #31	3.52	3.70	1.05
Ingot B / Wafer #29	3.38	3.54	1.05
Ingot C / Wafer #13	1.67	1.80	1.07

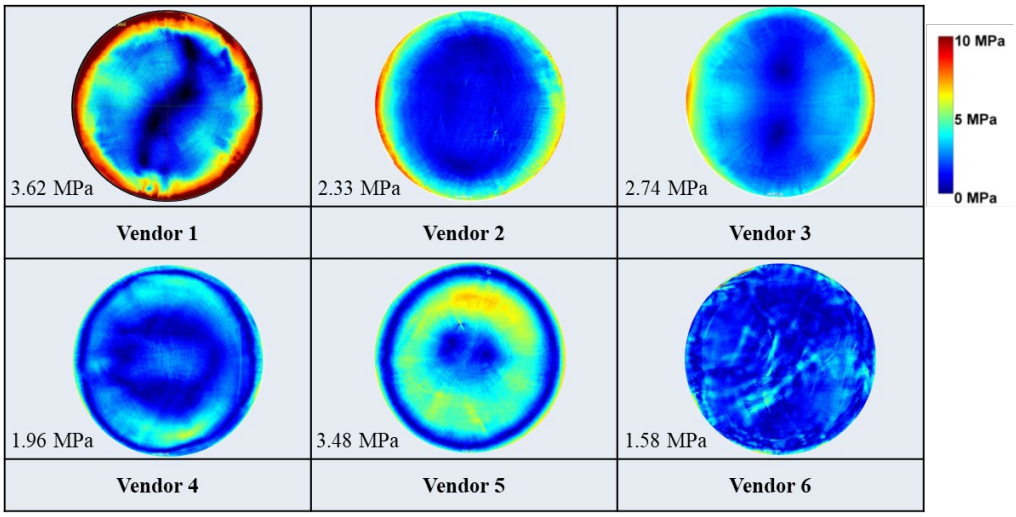

Fig. 2. Photoelastic stress distributions of representative 200 mm 4H-SiC wafers from six vendors (one wafer per vendor). Color scale indicates stress levels from 0 MPa (blue) to 10 MPa (red). Average values for each map are also indicated.

In order to further understand the nature of the stress pattern variation, the stress is decomposed into radial and tangential components based on the optical axis orientation (shown in the white arrows in Fig. 3). It is well known that light propagating along the c-axis of a stress-free 4H-SiC crystal exhibits no birefringence, as the ordinary and extraordinary refractive indices are equal, resulting in isotropic optical behavior due to the crystal's axial symmetry [8]. However, when mechanical stress is applied to 4H-SiC, the crystal lattice becomes distorted, breaking its axial symmetry and inducing birefringence, as the refractive indices for ordinary and extraordinary rays diverge, leading to polarization-dependent optical behavior.

The stress components along the radial (σ_r) and tangential (σ_t) directions of the wafer are derived from the principal stresses (σ_1, σ_2) along the birefringence axes, using the angle θ between the fast birefringence axis and the radial direction, given by the following equations [9]:

$$\sigma_r = \sigma_1 cos^2\theta + \sigma_2 sin^2\theta, \tag{2a}$$

$$\sigma_t = \sigma_1 sin^2\theta + \sigma_2 cos^2\theta, \tag{2b}$$

$$\tau_{rt} = (\sigma_2 - \sigma_1) sin\theta cos\theta. \tag{2c}$$

Since photoelastic measurements can only determine the absolute difference between σ_1 and σ_2, we assume $\sigma_2 \approx 0$ to simplify the calculation. Since $\sigma_1 > \sigma_2$ and $\sigma_2 \approx 0$, σ_1 represents a tensile stress. Furthermore, as the measured θ values in our samples are close to 0° or 90°, the equations can be approximated as:

$$\sigma_r \approx \sigma_1 cos\theta, \tag{3a}$$

$$\sigma_t \approx \sigma_1 sin\theta, \tag{3b}$$

$$\tau_{rt} \approx 0. \tag{3c}$$

The tangential tensile stress maps in Fig. 3 for both symmetric and asymmetric wafers exhibit a pronounced ring-like distribution at the wafer periphery (red, up to 20 MPa), tapering to the center (dark blue, near 0 MPa), suggesting that the tangential stress is not the primary factor for the asymmetry. It is speculated that during the cooling phase of crystal growth, a uniform peripheral contraction occurs that generates the tangential tensile stress to balance central expansion.

However, the radial tensile stress maps highlight the key difference: the symmetric pattern (top right figure) shows negligible radial stress throughout (near 0 MPa, average 0.416 MPa). In contrast, the asymmetric pattern (bottom right figure) exhibits significant radial tensile stress in the central region (average 1.513 MPa), reflecting anisotropic lattice bending or cooling irregularities that disrupt radial equilibrium and introduce non-uniform stress distribution. These contrasts underscore that the symmetric profile arises from optimized crystal growth with uniform thermal fields, while asymmetric profile, potentially stemming from uneven growth or cooling process or imperfect seed quality, manifests primarily through radial stress variations, elevating risks of multiplication of BPDs or cracking.

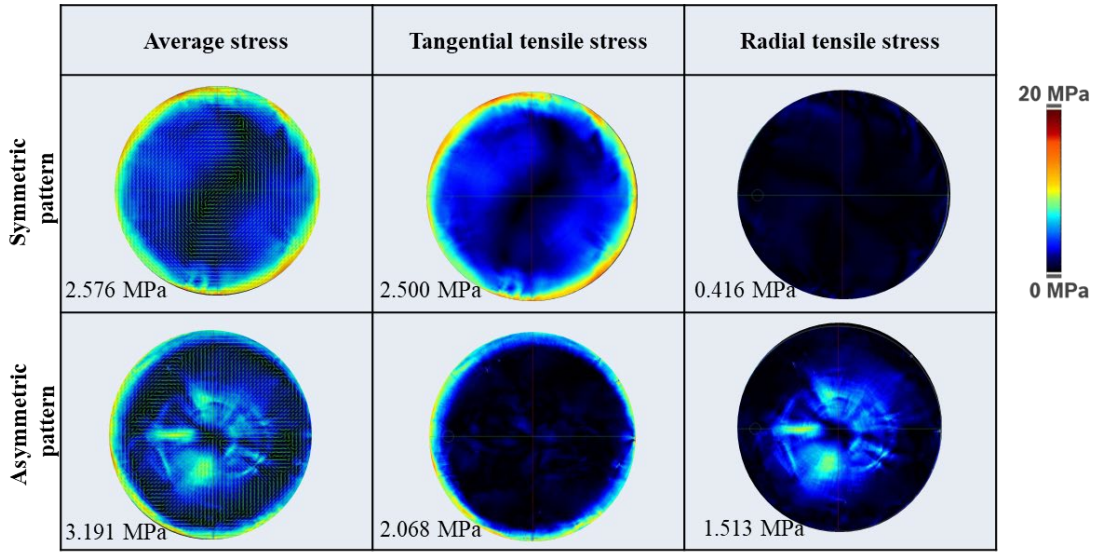

Fig. 3. Comparison of stress mapping in 200 mm SiC wafers with symmetric (top row) and asymmetric (bottom row) stress patterns. From left to right: average stress, tangential tensile stress, and radial tensile stress. The arrows in the average stress maps represent the direction of the fast birefringence axis, which also corresponds to one of the principal stress directions. Average values for each map are also indicated.

Incoming Wafer Warpage Inspection and Stress Correlation. Figure 4 illustrates a comparison of bow and warp measurements for identical 200 mm SiC wafers using E+H metrology with 2-rod support and FRT metrology with 3-point support. The FRT results consistently show significantly higher bow and warp values, primarily due to increased gravitational deformation under the 3-point support configuration. This setup subjects the wafer to greater gravitational loading, resulting in more pronounced bending. Notably, all bow values recorded by FRT are negative, indicating a consistent downward curvature and underscoring the sensitivity of wafer geometry to support mechanics and measurement conditions. In contrast, the E+H metrology system provides more stable support, with its 2-rod configuration positioned closer to the wafer center, effectively lowering gravitational effects. As a result, bow values remain near zero and warp values are lower compared to those measured by FRT.

Finally, to establish a reliable monitoring method for incoming 200 mm 4H-SiC wafers, we investigated the correlation between residual mechanical stress and various warpage parameters measured by either FRT metrology tool or E+H metrology tool. Interestingly, we found that only the warpage parameters significantly influenced by gravitational deformation, i.e., those measured using the FRT tool, showed a meaningful correlation with wafer stress. In contrast, bow and warp values obtained using the E+H tool with fewer gravitational effects, exhibited insufficient variation across wafers with different stress levels, making it difficult to establish a clear correlation.

The influence of gravity on wafer warpage measurements has been extensively discussed in the silicon industry [2-3, 10]. As an external force, gravity induces additional bending in the wafer, analogous to the mechanical deformation caused by process-induced stress during device fabrication. The effect of gravity also depends on the wafer's intrinsic curvature: it enhances bending in concave wafers and reduces it in convex wafers. To characterize this gravity-induced deformation, we reference the "z_gravity" concept described in SEMI standard MF1390-0218 for silicon wafers, introducing the term "sag value" in this paper [2].

The sag value is defined as the average of bow measurements taken with the wafer oriented both Si-face up and C-face up, using the FRT tool with 3-point support. Mathematically, it is expressed as:

$$Sag = \frac{bow_{Si-up} + bow_{C-up}}{2}, \quad (4)$$

where $bow_{Si\text{-}up}$ and $bow_{C\text{-}up}$ refer to the three-point bow values taken with the Si-face and C-face facing upward, respectively. This method captures the full extent of gravitational influence on wafer warpage. Unlike single-side bow measurements (typically Si-face up), the sag value provides a more comprehensive representation of the wafer's bending behavior, accounting for both orientations. This dual-side approach enables more effective screening of wafers with different shapes and stress profiles.

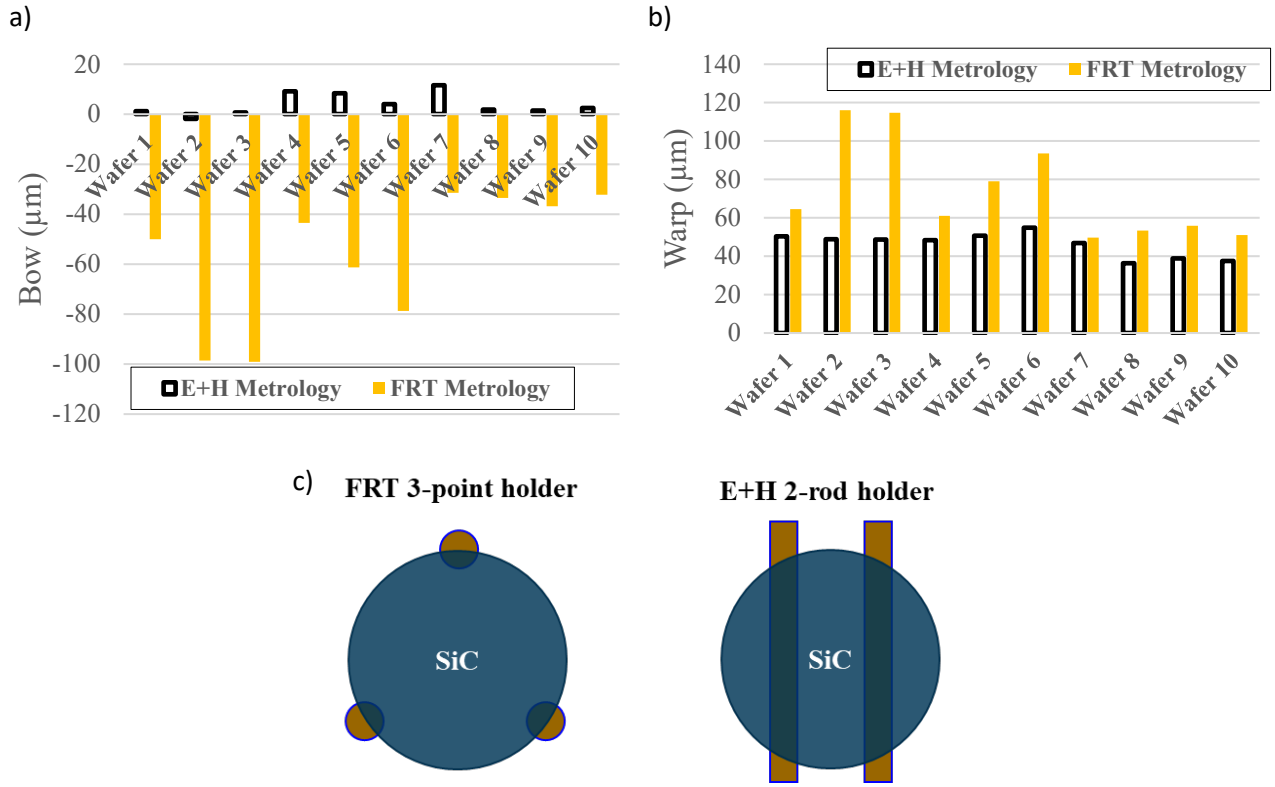

Fig. 4. Comparison of (a) bow and (b) warp measurements for identical 200 mm 4H-SiC wafers using the FRT metrology tool with a 3-point holder and the E+H metrology tool with a 2-rod holder; (c) schematic illustration of the 3-point and 2-rod holder configurations.

Figure 5(a)–(c) illustrates the correlation between absolute sag value and stress in 200 mm 4H-SiC wafers. The dataset is divided into two groups based on the typical stress patterns identified in Fig. 3. Blue circles represent wafers with symmetric, ring-like stress patterns, while orange squares correspond to wafers exhibiting asymmetric stress distributions.

In Fig. 5(a), two distinct correlation trends are observed: for a given sag value, wafers with asymmetric stress patterns tend to exhibit higher average stress than those with symmetric patterns. As discussed previously, the stress components can be decomposed into radial and tangential tensile stresses. In wafers with symmetric stress patterns, the stress is primarily tangential and concentrated near the wafer periphery. In contrast, wafers with asymmetric stress patterns show significant radial tensile stress concentrated near the wafer center, which contributes comparably to the overall stress. This distinction explains why, in Fig. 5(b), a unified trend between sag value and tangential tensile stress is observed, regardless of stress pattern type. Conversely, Fig. 5(c) shows no significant correlation between sag value and radial tensile stress for either group, suggesting that radial stress has a limited influence on sag. While the underlying mechanism remains under investigation, we hypothesize that the spatial distribution of stress components—particularly a peripheral tangential field—governs gravity-induced bending by constraining basal-plane curvature. Accordingly, our future work will (i) develop a mechanics-based model that couples the measured stress components to the observed sag, and (ii) directly correlate the Fig. 5(b) metric (tangential tensile stress) with BPD distributions via molten KOH etching and/or X-ray topography on the same 200 mm wafers, to

establish quantitative stress–dislocation–warpage relationships. This is consistent with prior observations connecting residual stress, BPD distributions, and basal-plane bending in SiC growth [11].

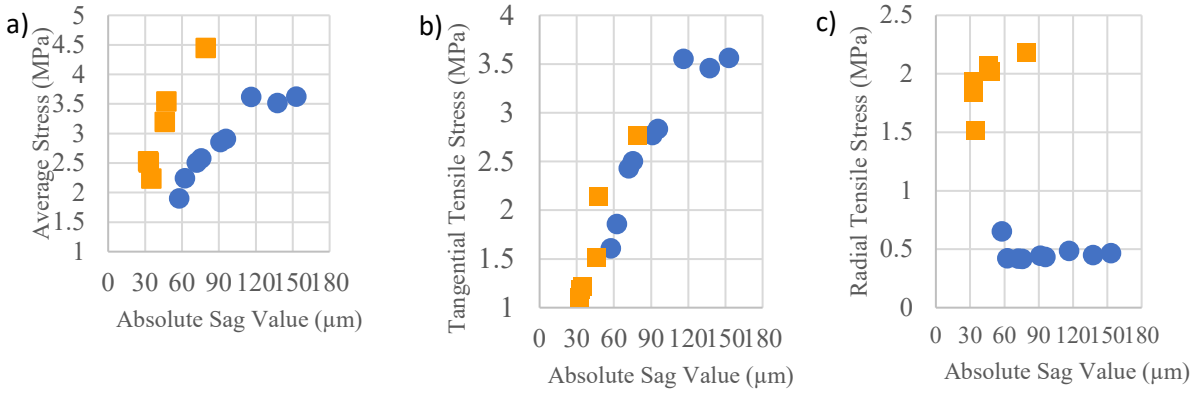

Fig. 5. Correlation between absolute sag value and stress in 200 mm SiC wafers. (a) Average stress vs. sag value; (b) Tangential tensile stress vs. sag value; (c) Radial tensile stress vs. sag value. Blue circles represent wafers with symmetric ring-like stress patterns, while orange squares indicate asymmetric stress patterns.

Summary

In this study, we investigated the mechanical stress and warpage behavior of 200 mm bare 4H-SiC wafers. Photoelastic measurements were employed to quantify residual stress, revealing significant variation among wafers from different vendors—an indication of differing levels of process maturity in crystal growth and wafering. The stress distributions were classified into two dominant types: symmetric and asymmetric. By decomposing the stress into tangential and radial components based on the optical axis orientation, we attributed these patterns to distinct stress mechanisms. In the analysis of wafer warpage, we demonstrated that the metrology setup—particularly the support method—plays a critical role in the measured bow and warp values due to gravitational deformation. To better capture this effect and correlate it with residual stress, we introduced the sag value as a representative metric for gravity-induced wafer bending. Our results show a clear correlation between sag value and average stress, with distinct trends for symmetric and asymmetric stress patterns. Interestingly, tangential tensile stress exhibited a unified correlation with sag value, independent of stress pattern type, while radial tensile stress showed no significant correlation. These findings suggest that warpage measurements influenced by gravity, such as those captured by the sag value, can serve as an effective and non-destructive method for monitoring the mechanical properties of incoming SiC wafers.

Acknowledgement

We gratefully acknowledge Dr. Christian Kranert and M. Sc. Paul Wimmer from Fraunhofer IISB Germany for the insightful discussions that inspired this work. The results are part of IPCEI ME/CT project which is supported by the Federal Ministry for Economic Affairs and Energy on the basis of a decision by the German Parliament, by the Ministry for Economic Affairs, Labor and Tourism of Baden-Württemberg based on a decision of the State Parliament of Baden-Württemberg, the Free State of Saxony on the basis of the budget adopted by the Saxon State Parliament, the Bavarian State Ministry for Economic Affairs, Regional Development and Energy and financed by the European Union - NextGenerationEU.

References

[1] Information on https://www.bosch-semiconductors.com/stories/silicon-carbide-chip-production-preparing-for-the-future/.

[2] SEMI MF1390-0218, Semiconductor Equipment and Materials International (2023).

[3] SEMI 3D12-1020, Semiconductor Equipment and Materials International (2015).

[4] E. Gamarts, P. Dobromyslov, V. Krylov, S. Prisenko, E. Jakushenko, V. I. Safarov, Characterization of stress in semiconductor wafers using birefringence measurements, J. Phys. III 3 (1993) 1033.

[5] Information on https://www.raphaeloptech.com/.

[6] Information on https://ilis.de/en/products/strainscope/.

[7] M. Herms, G. Irmer, S. Spira, M. Wagner, The photoelastic constant of (0001) 4H silicon carbide determined by scanning infrared polariscopy, Phys. Status Solidi A 218 (2021) 2100198.

[8] M. Fukuzawa, K. Kanamoto, Photoelastic characterization of residual strain distribution in commercial off-axis SiC substrates, J. Electron. Mater. 49 (2020) 5161–5166.

[9] J.M. Gere, B.J. Goodno, Mechanics of materials, 7th ed., Cengage Learning, 2009, pp.538-566.

[10] H. Liu, X. Zhu, R. Kang, Z. Dong, X. Chen, Three-point-support method based on position determination of supports and wafers to eliminate gravity-induced deflection of wafers, Precision Eng. 46 (2016) 339–348.

[11] T. Ailihumaer, H. Peng, B. Raghothamachar, M. Dudley, G. Chung, I. Manning, E. Sanchez, Relationship between basal plane dislocation distribution and local basal plane bending in PVT-grown 4H-SiC crystals, J. Electron. Mater. 49 (2020) 3455–3464.